Australian Earthquake Engineering Society
2024 National Conference, 21-23 November 2024
Adelaide, South Australia

An Updated Ground Motion Model for Australia Developed Using Broadband Ground Motion Simulations

Jeff Bayless[1] and Paul Somerville[2]

1. AECOM, Los Angeles, jeff.bayless@aecom.com
2. AECOM, Los Angeles, paul.somerville@aecom.com

Abstract

Changes to seismic hazard models with time reflect our increasing knowledge of earthquake source and ground motion characteristics in Australia. Because considerable strong ground motion recordings have been collected and analysed in Australia in recent years, it is important to update the ground motion models (GMMs) which underpin the seismic hazard results and, ultimately, drive the design ground motions in future engineering standards and guidelines. The Somerville et al. (2009; Sea09) GMMs for Australia are due for improvement by taking advantage of these ground motions recorded in the past decade-plus. This paper describes a ground motion model which updates Sea09.

Our updated GMM uses broadband strong motion simulations to account for earthquake source and crustal structure properties of Australia. The simulations are validated with data recorded in Cratonic and non-Cratonic Australia (provided by Geoscience Australia; Ghasemi and Allen, 2021) and use contemporary methods (Graves and Pitarka, 2015). The validations compare attenuation, goodness of fit, and spectral shapes of the simulated ground motions with those recorded in Australian earthquakes. Large suites of forward simulations are used to model the scaling to larger earthquake magnitudes that typically control design ground motions but for which no Australian data are available. These simulations are used to constrain the magnitude scaling, depth scaling, near-source saturation, and distance scaling components of the GMM.

Recently recorded ground motions in Australia have revealed that the Cratonic and non-Cratonic region data show minimal differences in magnitude and distance scaling and can have similar spectral shapes depending on the region, with most differences attributed to source effects (Bayless et al., 2023). As a result, the Cratonic and non-Cratonic versions of our updated GMM share magnitude scaling and geometric spreading models. The Cratonic and non-Cratonic GMMs differ in their anelastic attenuation components, which models deviations from the geometric spreading attenuation, and also differ in their high frequency source spectra; these account for the differences in source and crustal structure between regions. Two source effects related to earthquake depth are modelled: the effects of surface (R_g) waves from shallow events, impacting longer periods, and the effects of energetic buried ruptures, impacting short periods. The model is for the median and standard deviation of the horizontal component of response spectral acceleration.

Keywords: Ground motion models, ground motions simulations, seismic hazard

1 Introduction

One critical component of a seismic hazard assessment (SHA) is the selection of ground motion models (GMMs), because the SHA results are highly dependent on these models. The Somerville et al. (2009; Sea09) GMMs for Australia were based on ground motion simulations, and then checked for consistency with the recorded ground motions of the moment magnitude (**M**) 4.47 Thompson Reservoir earthquake of 1996. In the course of the National Seismic Hazard Assessment (NSHA18; Allen et al., 2018), Geoscience Australia assessed the performance of existing ground motion models in predicting recorded ground motions in Australia (Ghasemi and Allen, 2018); the Allen (2012) and Sea09 models were the only Australian models that were considered. Ghasemi and Allen (2018) demonstrated that Sea09 could be improved by taking advantage of ground motions recorded in the past decade-plus. The expectation of change in GMMs is embodied in Section 2.5 of the 2019 ANCOLD seismic guidelines, which states that it is unlikely that a SHA more than about 10 years old is reliable. Changes to seismic hazard models with time reflect our increasing knowledge of earthquake source and ground motion characteristics in Australia.

This paper describes how the Sea09 GMM has changed, and as a result how SHA results for engineering projects may be impacted. Comparisons with recently recorded ground motions in Australia have revealed that refinements to the distance and depth scaling components of the model provide a better fit to those data. This update also involves a large suite of earthquake ground motion simulations; these are validated using the recorded ground motion data and are used to extrapolate the model to larger earthquake magnitudes that typically control design ground motions but for which no Australian data are available.

2 Earthquake Ground Motion Data

We compiled a Cratonic earthquake ground motion database including waveform data from Geoscience Australia (Ghasemi and Allen, 2021), who provided instrument corrected recordings for events occurring within Cratonic regions, and from IRIS (https://ds.iris.edu/wilber3/). We removed events with **M** less than 3.0, recordings with distance greater than 600 km, and those identified as clipped, with poor signal to noise ratio, or other artifacts. Recordings without both orthogonal horizontal components were also removed. The resulting database contains 536, homogeneously processed, ground motion records from 84 events recorded by 155 unique stations.

The Cratonic ground motion database includes three earthquakes with more than 80 records, these are the **M**3.91 event on 2019 May 30, the **M**4.71 event on 2019 May 30, and the **M**4.96 event on 2019 August 1. These three earthquakes were located within the Northern Australian Craton and were recorded by the temporary AusARRAY deployment (Gorbatov et al., 2020). The remaining 81 earthquakes in the database used in this study have fewer than 14 recordings within 600 km. There are 35 total events with $\mathbf{M} \geq 4.0$ and 33 events with $3.5 \leq \mathbf{M} < 4.0$. The 5%-damped, horizontal component pseudo-spectral accelerations (RotD50; Boore, 2010) are calculated from two-component band-passed acceleration time histories using the pyRotd python library (Kottke, 2018).

The cut-and-paste (CAP) method for retrieving earthquake source parameters (Zhao and Helmberger, 1994; Tan et al., 2010) breaks three-component data into regional P waves (*Pnl,* consisting of refractions along the crust–mantle interface, Pn, and the crustal P arrivals and

PmP along with various S segments at distances from 150 to 1400 km; Helmberger and Engen, 1980*)* and surface-wave segments, and models them separately, so imperfect 1-dimensional Green's functions can be effectively used to determine source parameters. We use the CAP method on nine of the 12 events listed in Table 1 to improve our estimates of **M**, focal depth, focal mechanism, and location, resulting in some differences between our source parameter estimates and those from the GA and global catalogues.

Table 1. Cratonic region earthquakes used in the GMM development. Metadata for EQIDs 13, 49, and 55 are from Ghasemi and Allen (2021).

EQID	M	Date	Epicenter Longitude (deg)	Epicenter Latitude (deg)	Hypocenter Depth (km)	Strike, Rake, Dip (deg)	Region	No. of Usable 2-comp recs
61	4.96	2019-08-01	133.916	-19.7647	2	302, 47, 79	North. Aus. Craton	98
59	4.71	2019-05-30	131.85876	-21.28147	5	103, 59, 14	North. Aus. Craton	83
60	3.91	2019-05-30	131.92337	-21.32752	4	101, 64, 3	North. Aus. Craton	85
58	5.34	2018-11-08	116.78733	-34.42316	9^	151, 90, 52	Yilgarn Craton	13
53	4.90*	2018-09-16	116.78	-34.43	7^	347, 53, 44	Yilgarn Craton	6
44	4.91	2016-07-08	122.511	-32.458	5	331, 37, 59	Yilgarn Craton	6
13	4.6	2002-03-30	117.049	-30.519	0.8	-,-,-	Yilgarn Craton	8
55	4.54	2018-10-12	116.79882	-34.39522	5.8	-,-,-	Yilgarn Craton	8
49	4.13	2017-01-03	118.455	-30.609	10	-,-,-	Yilgarn Craton	9
72	4.39	2010-06-05	136.796	-33.5949	23	0, 62, 51	Gawler Craton	5
82	3.53	2018-07-01	136.7729	-33.618	23	209, 38, 51	Gawler Craton	5
83	4.41	2018-11-21	136.923	-33.2585	33	319, 32, -83	Gawler Craton	5
84	5.32	2021-11-13	119.8416	-21.1301	34.9	-,-,-	Pilbara Craton	12

*The global CMT **M** and depth are 5.3 and 12 km
^More appropriate hypocentral depths may be in the range 2-4 km; Clark et al. (2020)

Table 2. Non-Cratonic region earthquakes used in the GMM development.

EQID	M	Date	Epicenter Longitude (deg)	Epicenter Latitude (deg)	Hypocenter Depth (km)	No. of usable response spectra
1001	4.4	2007-12-26	138.383	-32.086	16.4	12
1002	4.5	2010-06-05	136.719	-33.589	22.4	6
1003	5.1	2012-06-19	146.29	-38.259	18.06	25
1004	3.6	2018-07-01	136.679	-33.606	10	10
1005	3.7	2018-11-21	136.846	-33.361	10	9
1006	6.5	2019-07-14	120.295	-18.262	20	1
1007	4.2	2020-05-14	138.802	-33.711	10	8
1008	5.9	2021-09-21	146.348	-37.492	10	28
1009	4.7	2021-10-08	141.021	-35.408	1.7	13
1010	4.3	2023-03-22	139.592	-32.785	8.8	12
1011	4.4	2023-06-29	146.313	-37.502	7.4	29
1012	3.9	2023-09-08	150.733	-34.153	2.4	14
1013	4.8	2023-10-21	143.489	-38.651	7.2	17

The non-Cratonic ground motion database includes response spectra and metadata only and was provided by Geoscience Australia (Trevor Allen, personal communication) at our request. From the data provided by Geoscience Australia, we identified the 13 events listed in Table 2 to be used for the GMM development. These include the 2021 **M**5.9 Woods Point and 2012

M5.1 Moe earthquakes in Victoria, and one recording of the 2019 **M**6.5 earthquake off the Kimberley coast.

3 Earthquake Ground Motions Simulations

Ground motion simulations are used to model the scaling to larger earthquake magnitudes that typically control design ground motions but for which no Australian data are available. These simulations are used to constrain the magnitude scaling, depth scaling, near-source saturation, and distance scaling components of the GMM.

The first phase of using the earthquake ground motion simulations is validation against the available data from Section 2. The validation phase is critical to establish confidence in the simulations and their input parameters, such as the seismic velocity models used to develop Green's Functions. The validation efforts involve simulating the well-recorded earthquakes in the region and comparing the simulated waveforms, response spectra (including attenuation with distance and spectral shape), and finally with a goodness-of-fit calculation to determine if there is any period-dependence in the mean bias of the simulations with respect to the data. The validation phase is described in Bayless et al. (2023) and Bayless et al. (2022).

The second simulation phase involves performing simulations for suites of scenario events with a range of magnitudes, source depths, and kinematic source realizations to develop a simulated ground motion database. Several components of the GMM are based on this suite of simulations. This phase is described in Section 3.2 of this paper.

3.1 Simulation Methodology

We use the hybrid broadband ground motion simulation methodology of Graves and Pitarka (2015; 2014; 2010; 2004; GP15) as implemented on the Southern California Earthquake Center Broadband Platform, version 22.4 (SCEC BBP; Maechling et al., 2015). The GP15 method combines a deterministic approach at low frequencies (f<1 Hz) with a semistochastic approach at high frequencies (f>1 Hz), where the broadband (0-10 Hz) response is obtained by summing the separate responses in the time domain using matched filters centred at 1 Hz. In GP15 the fault rupture is represented kinematically and incorporates spatial heterogeneity in slip, rupture speed, and rise time by discretising an extended finite-fault into a number of smaller subfaults. The GP15 prescribed slip distribution is constrained to follow an inverse wavenumber-squared fall-off and the average rupture speed is set at a fraction of the local shear-wave velocity, which is then adjusted such that the rupture propagates faster in regions of high slip and slower in regions of low slip. At low frequencies (f<1 Hz), the GP15 methodology contains a theoretically rigorous representation of fault rupture and wave propagation effects and attempts to reproduce recorded ground motion waveforms and amplitudes by summing the response for many point sources distributed across each subfault. At high frequencies (f>1 Hz), GP15 uses a stochastic representation of source radiation, which is combined with a simplified theoretical representation of wave propagation and scattering effects for each subfault.

Graves and Pitarka (2015) extended their broadband simulation method from active region crustal earthquakes to earthquakes in stable continental regions based on findings from Somerville et al. (2009), Leonard (2010; 2014), Beresnev and Atkinson (2002), and with calibration using three eastern North America earthquakes. The modifications included:

increasing the average rise time, reducing the average corner frequency, increasing the high frequency stress parameter, using the Leonard (2010; 2014) magnitude-area scaling relations, changing the high frequency attenuation (through kappa and Q models), changing the background rupture speed, and removing the shallow and deep weak zones from the rupture characterisation (Graves and Pitarka, 2015).

3.2 Forward Simulations

A large suite of forward simulations was performed using the Center for Advanced Research Computing (CARC) resources at the University of Southern California. Tables 3 and 4 list the parameters used to define the earthquake scenarios for the Cratonic and non-Cratonic simulations, respectively. The scenarios are all reverse-faulting earthquakes with **M** ranging from 5.0 to 7.75 with rupture dimensions from the Leonard (2010) magnitude-area scaling relations. For each magnitude, we specified one scenario which breaks the ground surface, even though small earthquakes do not usually break the surface in tectonically active regions (Wells and Coppersmith, 1994), and at least one scenario nucleating deeper in the crust. As indicated in Table 1 and described by King et al. (2019) and Yang et al. (2021), earthquakes in Cratonic regions of Australia tend to have shallow hypocentres and rupture the ground surface, even for magnitudes 5.0 and smaller (Dawson et al., 2008). The 2021 Marble Bar earthquake in the Pilbara Craton and earthquakes near Cleve, Eyre Peninsula in the Gawler Craton are exceptions, occurring at depths of 30 km or more. Accordingly, for the Cratonic scenarios, two depths were used per magnitude: a surface rupturing earthquake, and one with depth to bottom of rupture at 30km. For non-Cratonic simulations, we used a range of earthquake depths for each magnitude. Ten realisations of the finite-fault source model with randomly located hypocentres are used for each scenario.

Simulation stations (locations where the ground shaking time histories are saved) were oriented in rupture distance (R_{rup}) bands surrounding the finite faults, with 20 stations per band surrounding the rupture at the following rupture distances: 0.1, 0.2, 0.3, 0.5, 1, 2, 3, 5, 7, 10, 20, 30, 50, 70, 100, 200, 300, 500, and 600 km. In cases where the earthquake depth is greater than any of these R_{rup} distances, the subset of possible distance bands was used. Using the same R_{rup} bands for each scenario, regardless of the depth, allows for isolation of depth effects, as described in Section 4.4.

Table 3. Parameters of the Cratonic region earthquake scenarios used in the GMM development.

M	Rupture Length, L (km) from Leonard (2010)	Down-Dip Rupture Width, W (km) from Leonard (2010)	Dip (deg)	Depth to top of rupture, Ztor (km)	Depth to Bottom of Rupture (km)
5.00	2.6	2.5	45	0.0	1.8
				28.2	30.0
5.50	5.1	4.0	45	0.0	2.8
				27.2	30.0
6.00	10.2	6.3	45	0.0	4.5
				25.5	30.0
6.50	20.3	10.0	45	0.0	7.1
				22.9	30.0
7.00	40.6	15.9	45	0.0	11.2
				18.8	30.0
7.50	80.9	25.2	45	0.0	17.8
				12.2	30.0
7.75	114.3	31.7	45	0.0	22.4

Table 4. Parameters of the non-Cratonic region earthquake scenarios used in the GMM development.

M	Rupture Length, L (km) from Leonard (2010)	Down-Dip Rupture Width, W (km) from Leonard (2010)	Dip (deg)	Depth to top of rupture, Ztor (km)	Depth to Bottom of Rupture (km)
5.00	2.8	3.5	45	0.0	2.5
				5.0	7.5
				10.0	12.5
				15.0	17.5
				20.0	22.5
				25.0	27.5
5.50	5.7	5.6	45	0.0	3.9
				2.5	6.4
				5.0	8.9
				7.5	11.4
				10.0	13.9
				15.0	18.9
				20.0	23.9
				25.0	28.9
6.00	11.3	8.8	45	0.0	6.2
				5.0	11.2
				10.0	16.2
				15.0	21.2
				20.0	26.2
6.50	22.6	14.0	45	0.0	9.9
				5.0	14.9
				10.0	19.9
				15.0	24.9
				20.0	29.9
7.00	45.1	22.2	45	0.0	15.7
				5.0	20.7
				10.0	25.7
				15.0	30.7
7.50	90.0	35.1	45	0.0	24.8
				5.0	29.8

The simulations use the Green's functions described in Bayless et al. (2022) and are for a reference V_{S30} condition of 760 m/s with no site response. The products of the simulations are ground motion time histories and response spectra. All the simulations, including input files and output files, are available (see Data and Resources). In total, there are 104,000 simulated three-component ground motion time histories from 410 simulated earthquakes.

4 Ground Motion Model

Because the Sea09 model works well for earthquake ground motions in Australia (e.g. Hoult et al., 2021; Allen et al., 2023, Tables 7.5 and 7.6), our initial preference was to make minor modifications to the model in this GMM update. However, the simulations indicated significant differences in magnitude scaling that we determined would be difficult to incorporate with minor modifications to Sea09. Additionally, we wanted to adopt an existing model for hanging wall effects and identified the Donahue and Abrahamson (2014) model as the best option. The Donahue and Abrahamson (2014) model is designed to adjust a model based on the the rupture distance metric (R_{rup}) and is not compatible with a Joyner-Boore distance (R_{JB}) based model, which Sea09 uses. Because of these factors, we chose to develop a completely new model rather than a modification to Sea09, by adopting the formulation of the magnitude and distance scaling from Abrahamson et al. (2014; ASK14 hereafter).

The median GMM has components for magnitude scaling, distance scaling, and earthquake depth scaling which were developed from the simulations. We have also adopted model components from others: V_{S30} scaling, basin depth scaling, and hanging wall scaling, and the aleatory variability. Each of these model components is described in the following sections.

The simulation-based models were compared with the available data (Tables 1 and 2) using a mixed effects regression and we found that short period ground motions in non-Cratonic regions were being systematically under-estimated. We modified the leading coefficient (representing the mean spectral shape due to the energy radiated at the source) to account for this difference, so the GMMs are based on the combination of the scenario simulations and the data residual analyses. The Cratonic and non-Cratonic versions of our GMM share a functional form and differ only in their coefficient values. The magnitude scaling and geometric spreading coefficients are the same for both models. The Cratonic and non-Cratonic GMMs differ in their high frequency source spectra and differ in their anelastic attenuation components; these account for the differences in source and crustal structure between regions.

4.1 Model Form

The model for the RotD50 component of 5% damped spectral acceleration (units g) is:

$$ln(RotD50) = ln(RotD50)_{med} + \epsilon\sigma \quad (1)$$

in which σ is is the total aleatory variability and the standard normal random variable ϵ is the number of logarithmic standard deviations above or below the median. The median model is:

$$ln(RotD50)_{med} = f_M + f_P + f_S + f_{Z1.0} + f_{Ztor} + f_{HW} \quad (2)$$

in which each of the model components in Eq. 2 is described in the following sections.

4.2 Magnitude Scaling

To capture the effects of energy radiated at the source, the polynomial formulation for the magnitude scaling is adopted from ASK14:

$$\begin{aligned} f_M &= a_1 + a_5(\mathbf{M}\text{-}M_1) + a_8(8.5\text{-}M)^2 && \text{for } \mathbf{M} \geq M_1 \\ f_M &= a_1 + a_4(\mathbf{M}\text{-}M_1) + a_8(8.5\text{-}M)^2 && \text{for } M_2 \leq \mathbf{M} < M_1 \\ f_M &= f_M(\mathbf{M}=M_2) + a_6(\mathbf{M}\text{-}M_2) + a_7(M\text{-}M_2)^2 && \text{for } \mathbf{M} < M_2 \end{aligned} \quad (3)$$

where **M** is the moment magnitude and the magnitude scaling breaks are $M_2 = 5.0$ and period-dependent M_1 ranging between 6.75 and 7.25. All the magnitude scaling term coefficients were determined in the regression.

4.3 Distance Scaling

The path scaling formulation of ASK14 is used:

$$f_P = [a_2 + a_3(\mathbf{M}\text{-}M_1)]\ ln(R) + a_{17}R_{rup} \quad (4)$$

where $R=(R_{rup}^2+c_{4M}^2)^{1/2}$ with R_{rup} in km and c_{4M} is the additive distance term to represent the near-source amplitude saturation effects of the finite-fault rupture dimension as described in Abrahamson et al. (2014). The $ln(R)$ term models the magnitude-dependent geometric spreading and the term $a_{17}R_{rup}$ models anelastic attenuation and scattering effects.

4.4 Earthquake Depth Scaling

For source effects related to earthquake depth we have developed a new model which represents the effects of R_g waves from shallow events, impacting longer periods, and the effects of energetic buried ruptures, impacting short periods. This depth model is a polynomial of the form:

$$f_{Ztor} = d_1Z^3 + d_2Z^2 + d_3Z + d_4 \quad (5)$$

where $Z=min(Z_{tor},20)$ and d_1 through d_4 are period-dependent coefficients and Z_{tor} is the depth to the top of the rupture plane in km.

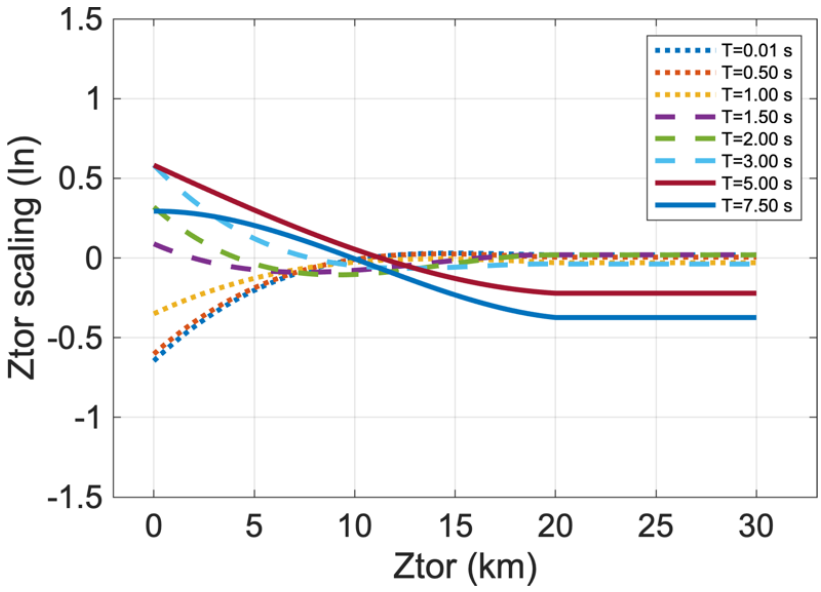

Figure 1. The earthquake depth (Z_{tor}) scaling model.

Somerville (2003) found that the short-period ground motions generated by earthquakes that do not have large shallow asperities are stronger than those of earthquakes that do. The simulations we performed, and the Z_{tor} scaling model derived from them, is consistent with this observation: the short periods (dotted lines) have lower ground motions for shallow sources and higher ground motions for deeper sources.

Somerville et al. (2009) found that a shallow low velocity layer overlying crystalline basement explained very dispersive R_g waves observed in recordings of shallow Australian earthquakes, noting that R_g is typically excited by events shallower than 3km (Saikia et al., 1998). As a result, the Sea09 Cratonic model includes a localised peak (or bump) in the predicted response spectra for periods of approximately 2-3 seconds due to the shallow earthquake source located in the high near-surface velocity structure. Our simulations are also consistent with this as shown in Figure 1; for shallow earthquakes the periods between about 1.5-3 sec (dashed lines)

have stronger ground motions. For periods longer than about 3 sec (solid lines) the simulations demonstrated decreasing ground motions with depth (down to about 20 km) at a given R_{rup}.

4.5 Adopted Median Model Components

We adopted the hanging wall effects model from Donahue and Abrahamson (2014) as implemented in ASK14, including the functional form and coefficients. This model is designed to modify a GMM based on R_{rup} and was calibrated based on simulations similar to those used in this paper and validated against the available data. The hanging wall model increases the short period ground motions for near-fault sites on the hanging wall side of the rupture using distance tapers to define the hanging wall region.

Models for V_{S30} scaling and $Z_{1.0}$ scaling are adopted from Boore et al. (2014), including the functional form and coefficients. The Boore et al. (2014) V_{s30} scaling model is described in Seyhan and Stewart (2014) and includes linear and non-linear components; this model has a reference V_{s30} (velocity at which the amplification is unity) of 760 m/s which is directly compatible with our simulation-based GMM. The $Z_{1.0}$ scaling is an adjustment to the base model to consider the effects of basin depth; it is based on the variation in $Z_{1.0}$ at a given site relative to the average $Z_{1.0}$ derived from V_{s30}. Until further data V_{s30} and $Z_{1.0}$ data are collected in Australia, we recommend using the default Boore et al. (2014) $Z_{1.0}$ value derived from V_{s30}, which turns off the $Z_{1.0}$ scaling component of the GMM.

4.6 Aleatory Variability Model

Models for the aleatory variability are adopted from Al Atik (2015), including models for the between-event standard deviation (τ), and total within-event standard deviation (ϕ). The total standard deviation in natural log units is calculated from these components using Eq. 6:

$$\sigma = \sqrt{\tau^2 + \phi^2} \tag{6}$$

4.7 Range of Applicability

The Cratonic and non-Cratonic GMMs are applicable for **M** 4.0-8.0, rupture distances from 0-300 km, and spectral periods 0.01-10 sec. The Boore et al. (2014) V_{S30} and $Z_{1.0}$ models are applicable for V_{S30} between 150-1,500 m/s and $Z_{1.0}$ between 0-3 km, and although we recommend using the same ranges, care should be taken to use these models until more V_{S30} and $Z_{1.0}$ data are collected in Australia. The upper limit of **M** 8.0 is beyond the largest simulation (**M** 7.75) and is based on extrapolation which we have checked and assumed to be reasonable. The GMM lower limit of **M** 4.0 is lower than the smallest magnitude of the forward simulations (**M** 5.0; Tables 3 and 4) and this is appropriate because the validation of the simulation methodology was performed using the data listed in Tables 1 and 2, which mostly ranges from **M** 4-5, and because the GMM verifications described in Section 5.1 were performed using the same data.

5 Model Performance

Figure 2 shows median response spectra from the models for the reference V_{S30} condition of 760 m/s, without $Z_{1.0}$ scaling, and for Z_{tor} = 0 km. In Figure 2, the solid lines are the non-Cratonic model, and the dotted lines are the Cratonic model. The different line colours are for different

earthquake **M** as indicated in the figure legend. The left and right panels of Figure 2 show response spectra for R_{rup} = 15 km and 150 km, respectively.

In Figure 2, the saturation in magnitude scaling at large **M**, especially at short periods and close distances, is apparent in the large spread in median spectra for small magnitudes, and very little sensitivity at larger **M**. Figure 2 also shows the **M**-dependence of the predominant period, with longer predominant period for increasing **M**. This figure also illustrates the differences between Cratonic and non-Cratonic models; for a given **M** and R_{rup}, the Cratonic model has higher short period (less than 0.2 sec) median response spectra, and the two models are more similar at longer spectral periods.

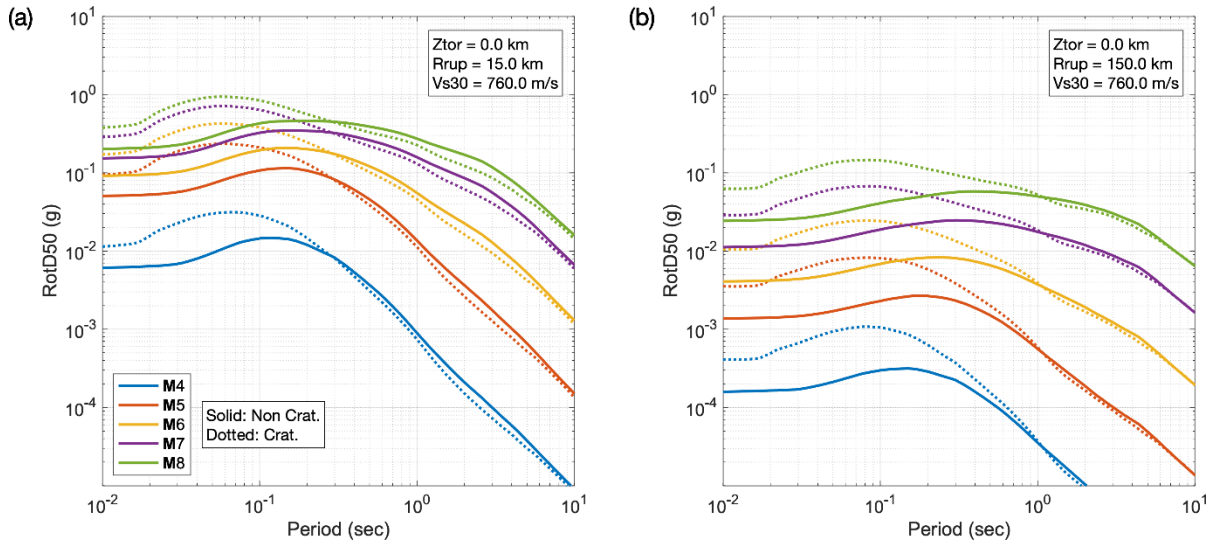

Figure 2. Median GMM response spectra for scenarios with Z_{tor}=0 km and the reference V_{S30} condition and without $Z_{1.0}$ scaling, for range of magnitudes (colours), for the Cratonic (dotted lines) and non-Cratonic (solid lines) models, at (a) R_{rup} of 15 km and (b) 150 km.

Figure 3 compares the short-period median response spectra versus R_{rup} with the Australian GMMs Allen (2012) and Sea09. This comparison uses Z_{tor} = 5 km and assumes sites are located on the footwall of the fault so there are no hanging wall effects. Sea09 is an R_{JB} model and in Figure 4 we use $R_{JB} = (R_{rup}^2 - Z_{tor}^2)^{1/2}$; this assumption is exact for sites on the footwall side of the rupture. We note that the Allen (2012) deep GMM is not strictly comparable to our models for 5 km depth but is still informative.

Figure 3 shows that the non-Cratonic model attenuates short-period ground motions more rapidly with increasing distance than the Cratonic model, due to differences in crustal Q (the $a_{17}R_{rup}$ term). The most significant differences in Figure 3 are due to how the attenuation with distance is modelled. Allen (2012) used a tri-linear geometrical attenuation featuring a transition zone between approximately 80-150 km in which the ground motions increase with distance, designed to account for direct waves joined by postcritical reflections from the Moho as originally proposed by Burger et al. (1987) and modelled by Allen (2012) and Allen et al. (2007). Sea09 represented the arrival of critical reflections from the lower crust with a decreased attenuation at 50 km but did not model an increase in ground motions with distance. Our analyses of the available data support a change in attenuation in this distance range as shown in Section 5.1, but our simulations support an attenuation model without a transition zone, such as the adopted ASK14 distance scaling model. Because of the limited quantity of

recorded data, and particularly our uncertainty in the site response adjustments, we elected to base the distance scaling component of our model primarily on the simulations.

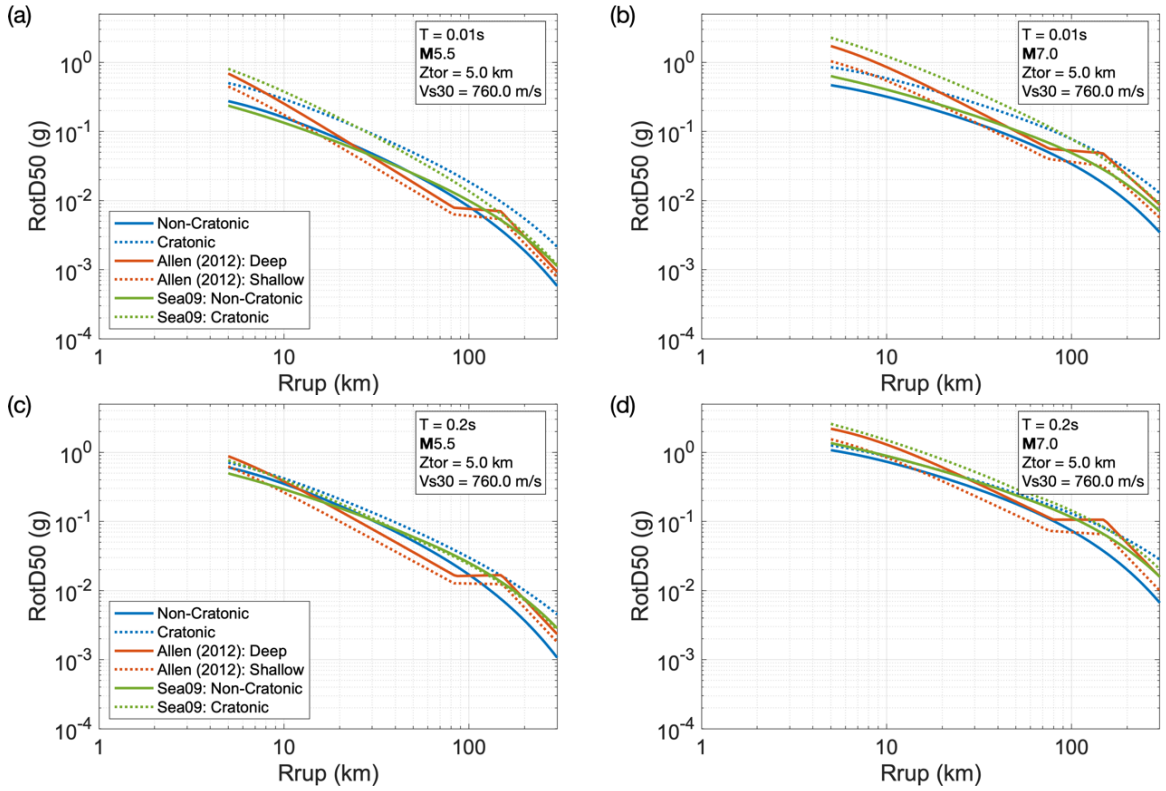

*Figure 3. A comparison of short-period median GMM response spectra for sites on the footwall side of the rupture and the reference V_{s30} condition, scenarios with Z_{tor} = 5 km: (a) T = 0.01 sec and **M**5.5, (b) T = 0.01 sec and **M**7.0, (c) T = 0.2 sec and **M**5.5, (d) T = 0.2 sec and **M**7.0.*

Figure 4 compares median ground motions versus distance for the hanging wall (solid lines) and footwall (dashed lines) sides of the fault. In Figure 4, R_x is the horizontal distance from the top edge of the rupture to the site measured perpendicular to the fault strike and W is the rupture down-dip width; all scenarios assume a dip of 45 degrees.

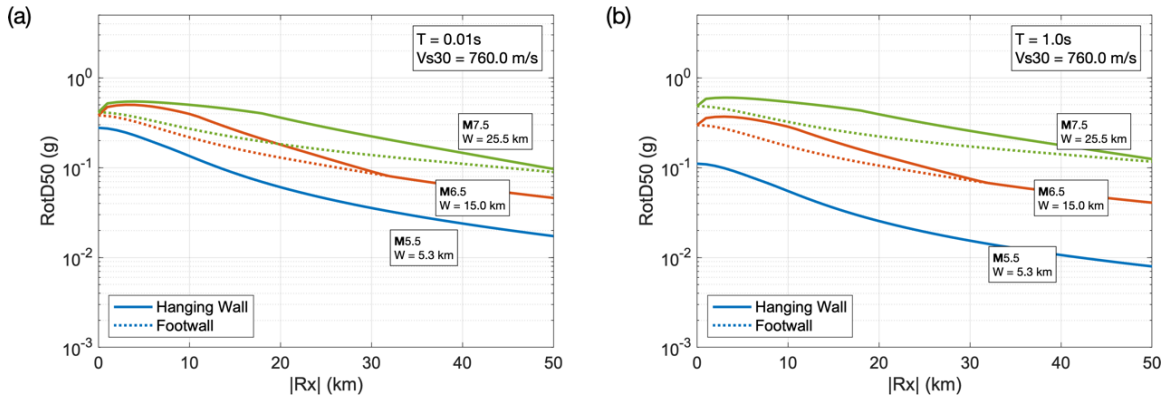

Figure 4. A comparison of hanging wall and footwall ground motions at: (a) T = 0.01 sec and (b) T = 1 sec. All sites use the reference V_{s30} condition, and all scenarios use Z_{tor} = 0 km.

Sea09 observed and modelled a localised peak around 1.5-2.0 seconds in the response spectra due to the R_g waves caused by a shallow low velocity layer in the Yilgarn Craton crust; this feature is present in the Sea09 Cratonic model for all earthquake depths (Figure 5). In our new model, the effects of R_g waves are represented in the depth scaling term which amplifies the long period ground motions for shallow earthquakes (Figure 5a) and de-amplifies them for deep earthquakes (Figure 5b). Relative to the Sea09 model, this long-period amplification is over a broader period range and so the spectral shape does not have a localised peak around 1.5-2.0 seconds. Figure 5 also shows that the revised Cratonic model has significantly different magnitude scaling from Sea09, especially at short spectral periods.

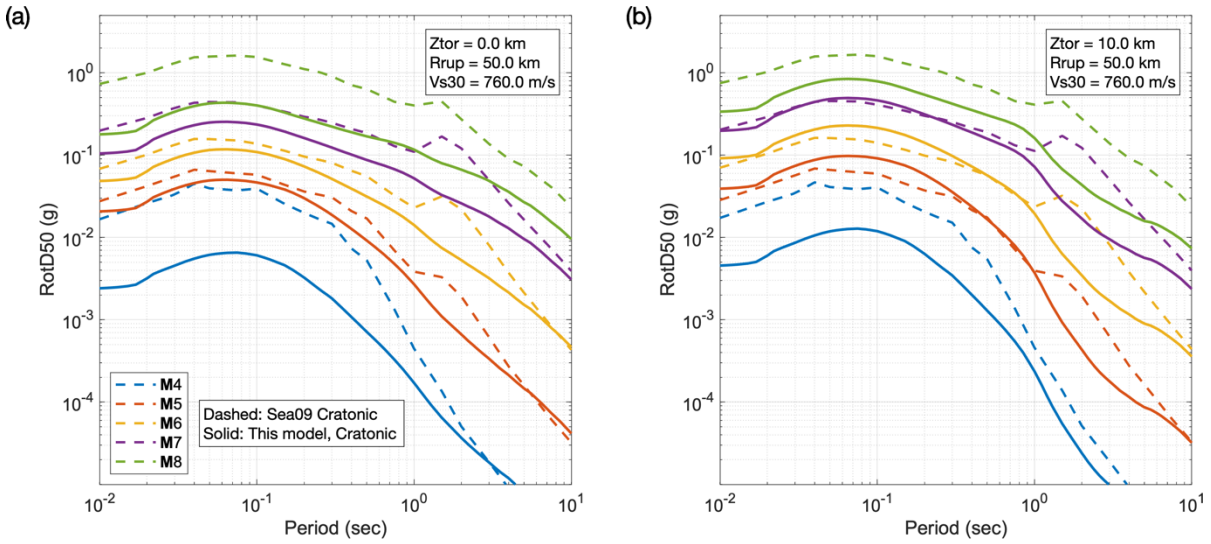

Figure 5. A comparison of footwall median GMM response spectra between Sea09 Cratonic (dashed lines) and the new Cratonic model (solid lines) at R_{rup} = 50 km, for (a) Z_{tor} = 0 km and (b) Z_{tor} = 10 km.

5.1 Comparisons with Data

We used the data described in Section 2 to check that the median GMM developed from the simulations is not biased with respect to magnitude, depth, and distance, e.g. Figure 6a. For a given spectral period and recording station, the residual is defined as the difference between the natural logarithm of the recorded spectral acceleration (data) and the natural logarithm of the median GMM. The uncertainties in V_{S30} values and in the site response adjustments are significant and could be reduced in the future with additional data collection or improved models; these sources of uncertainty were similarly identified and accepted in NGA-East (Goulet et al., 2021). We use a mixed-effects analysis to separate the residuals into between-event (δB_e) and within-event (δWE_{es}) residuals. Figure 6b and 6c show the between- and within-event residuals at T=1 sec.

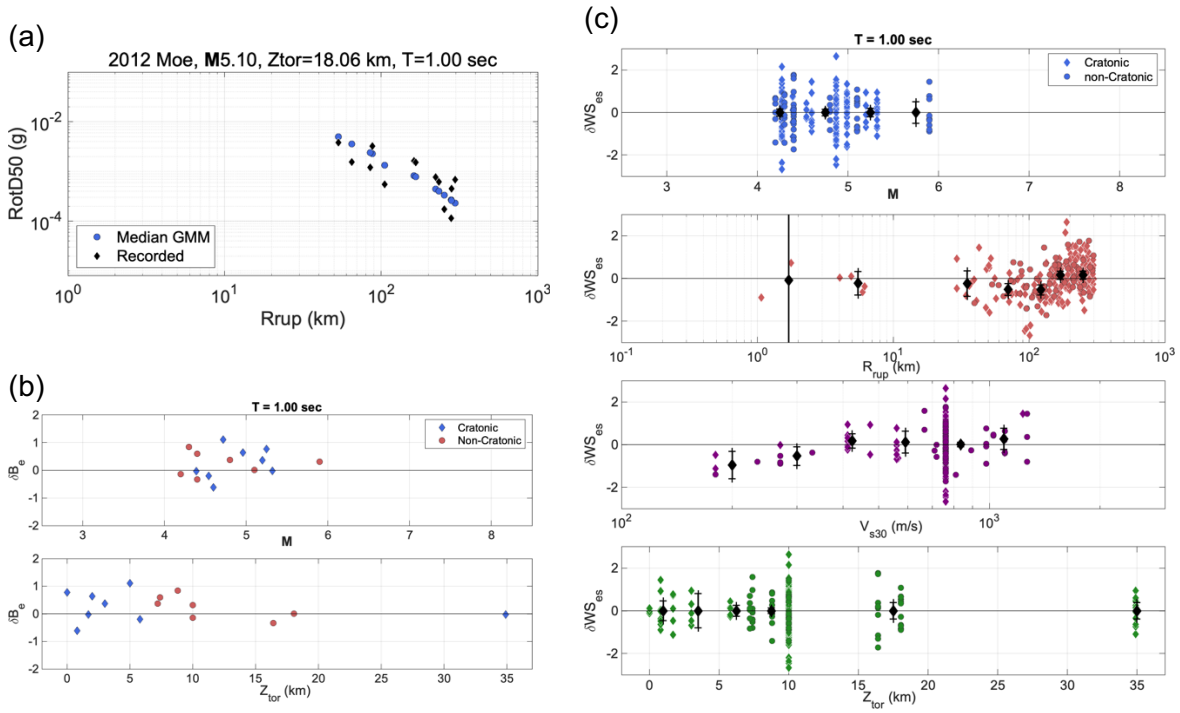

Figure 6. (a) Comparison between the model and data recorded in the 2012 Moe earthquake. (b) Between-event residuals for the complete dataset versus magnitude and depth, T=1 sec. (c) Within-event residuals versus magnitude, R_{rup}, V_{S30}, and Z_{tor} at T=1 sec.

6 Summary

This paper describes an updated GMM for the median and standard deviation of the horizontal component of response spectral acceleration for Cratonic and non-Cratonic regions of Australia. This update uses broadband strong motion simulations to account for the effects of earthquake source and crustal structure properties of Australia; these are validated using the available recorded ground motion data and are used to extrapolate the model to larger earthquake magnitudes that typically control design ground motions but for which no Australian data are available. We use the simulations to constrain the magnitude scaling, depth scaling, near-source saturation, and distance scaling components of the GMM. Two source effects related to earthquake depth are modelled: the effects of short period surface (R_g) waves from shallow events, impacting longer periods, and the effects of energetic buried ruptures, impacting short periods. We adopted the ASK14 model for hanging wall effects, the Boore et al. (2014) model for V_{S30} scaling, and the Al Atik (2014) global aleatory variability model.

The magnitude scaling and geometric spreading terms are the same for the Cratonic and non-Cratonic GMMs. The models differ in their anelastic attenuation components, which model deviations from the attenuation due to geometric spreading, and also differ in their high frequency source spectra derived from the simulations and validated by the data; these account for the differences in source and crustal structure between regions. The models provide adequate representations of the data and embody the differences in ground motions observed between Cratonic and non-Cratonic regions of Australia.

7 Acknowledgements

The authors acknowledge the Center for Advanced Research Computing (CARC) at the University of Southern California for providing computing resources that have contributed to the research results reported within this publication. URL: https://carc.usc.edu. We thank Geoscience Australia (in particular, Trevor Allen and Hadi Ghasemi) for making the Cratonic region ground motion and source data publicly available and for providing the non-Cratonic region response spectra. We thank Rob Graves and Arben Pitarka for providing input on the simulations and Fabio Silva for providing support with the SCEC Broadband Platform. We are grateful to one anonymous reviewer and again to Trevor Allen for his very thoughtful review.

8 Data and Resources

The DesignSafe repositories with the earthquake ground motion simulations described in Section 3.2 are available online at: doi.org/10.17603/ds2-w7qe-mh53 (Cratonic Simulations) and doi.org/10.17603/ds2-5pw1-s719 (Non-Cratonic simulations). Please contact the authors by email for the model coefficients and for programs implementing the model.

9 References

Abrahamson, N., W. Silva and R. Kamai (2014). Update of the AS08 Ground-Motion Prediction Equations Based on the NGA-West2 Data Set. Earthquake Spectra: August 2014, Vol. 30, No. 3, pp. 1025-1055.

Al Atik, L. (2015). NGA-East: Ground-Motion Standard Deviation Models for Central and Eastern North America. PEER Report 2015/07. Pacific Earthquake Engineering Center, University of California, Berkeley.

Allen, T. I., P. R. Cummins, T. Dhu, and J. F. Schneider (2007). Attenuation of ground-motion spectral amplitudes in southeastern Australia, *Bull. Seismol. Soc. Am.* **97,** 1279–1292, doi: 10.1785/0120060172.

Allen, T. I. (2012). Stochastic ground-motion prediction equations for southeastern Australian earthquakes using updated source and attenuation parameters, *Geoscience Australia Record 2012/69*, Canberra, pp 55.

Allen, T.I. (2018). The 2018 National Seismic Hazard Assessment for Australia: Data package: Maps and grid values. Geoscience Australia record 2018/33. Canberra, ACT, Australia

Allen, T., J. Griffin, M. Leonard, D. Clark and H. Ghasemi (2018). The 2018 National Seismic Hazard Assessment: Model overview. Record 2018/27. Geoscience Australia, Canberra. http://dx.doi.org/10.11636/Record.2018.027

ANCOLD (2019). Guidelines for Design of Dams and Appurtenant Structures for Earthquake.

Bayless J., P. Somerville, S. Condon, H.K. Thio, H. Ghasemi, T. Allen (2022). Updating the Somerville et al. (2009) Ground Motion Model for Cratonic Australia Using Broadband Ground Motion Simulations of Recently Recorded Cratonic Region Earthquakes. *Proc. of the 2022 Australian Earthquake Engineering Society National Conference.* 24-25 November 2022, Mount Macedon, Victoria, Australia.

Bayless J., P. Somerville, and H.K. Thio (2023). Ground motion modeling updates applicable to seismic hazard assessments for dams in Australia. *Proc. of the Australian National Committee on Large Dams Inc*. (ANCOLD) Conference. 25-27 October 2023, Cairns, Australia

Beresnev, I. A., and G. M. Atkinson (2002). Source parameters of earthquakes in eastern and western North America based on finite-fault modeling, Bull. Seis. Soc. Am. 92, 695–710.

Boore, D.M. (2010). Orientation-independent, nongeometric-mean measures of seismic intensity from two horizontal components of motion. Bulletin of the Seismological Society of America, Vol. 100, No. 4, pp. 1830-1835.

Boore, D. M., Stewart, J. P., Seyhan, E., and Atkinson, G. M. (2014). NGA-West2 equations for predicting PGA, PGV, and 5% damped PSA for shallow crustal earthquakes, Earthquake Spectra 30, 1057–1085.

Burger, R.W., P.G. Somerville, J.S. Barker, R.B. Herrmann, and D.V. Helmberger (1987). The effect of crustal structure on strong ground motion attenuation relations in eastern North America, Bull. Seism. Soc. Am., 77, 420-439.

Clark, D. J., S. Brennand, G. Brenn, M. C. Garthwaite, J. Dimech, T. I. Allen, and S. Standen (2020). Surface deformation relating to the 2018 Lake Muir earthquake sequence, southwest Western Australia: new insight into stable continental region earthquakes, *Solid Earth* **11,** 691–717, doi: 10.5194/se-11-691-2020.

Dawson, J., P. Cummins, P. Tregoning, and M. Leonard (2008). Shallow intraplate earthquakes in Western Australia observed by Interferometric Synthetic Aperture Radar, *J. Geophys. Res.* **113**, B11408, doi: 10.1029/2008JB005807.

Donahue, J. L., and Abrahamson, N. A. (2014). Simulation-based hanging wall effects, Earthquake Spectra 30, 1269–1284.

Ghasemi, H., and T. Allen (2021). Engineering ground-motion database for western and central Australia, Australian Earthquake Engineering Society 2021 Virtual Conference.

Ghasemi, H. and Allen, T. (2018). Selection and ranking of ground-motion models for the 2018 National Seismic Hazard Assessment of Australia: summary of ground-motion data, methodology and outcomes. Record 2018/29. Geoscience Australia, Canberra.

Gorbatov, A., K. Czarnota, B. Hejrani, M. Haynes, R. Hassan, A. Medlin, J. Zhao, F. Zhang, M. Salmon, H. Tkalcic, H. Yuan, M. Dentith, N. Rawlinson, A. Reading, B. Kennett, C. Bugden, and M. Costelloe (2020). AusArray: quality passive seismic data to underpin updatable national velocity models of the lithosphere; In, doi: 10.11636/135284.

Goulet, C.A, Bozorgnia, Y., Kuehn, N., Al Atik, L., Youngs, R.R., Graves, R.W. and Atkinson G.M. (2021). NGA-East Ground-Motion Characterization Model Part I: Summary of Products and Model Development. Earthquake Spectra, 37(S1): 1231–1282. https://doi.org/10.1177/87552930211018723

Graves R. W., Pitarka A. (2004). Broadband time history simulation using a hybrid approach, Proc. 13th World Conf. Earthq. Eng., Vancouver, Canada, paper no. 1098

Graves, R. W., Pitarka, A. (2010). Broadband ground-motion simulation using a hybrid approach, Bull. Seismol. Soc. Am. 100, 2095–2123, doi: 10.1785/0120100057.

Graves R. W., Pitarka A (2015). Refinements to the Graves and Pitarka (2010) Broadband Ground-Motion Simulation Method. Seismological Research Letters; 86 (1): 75–80. doi: https://doi.org/10.1785/0220140101

Helmberger, D. V., and G. R. Engen (1980). Modeling the long-period body waves from shallow earthquakes at regional ranges, Bull. Seism. Soc. Am. 70, 1699–1714.

Hoult, Ryan & Pascale, Adam & Jones, Abraham & Allen, Trevor. (2021). The MW 5.9 Woods Point Earthquake: A Preliminary Investigation of the Ground Motion Observations.

Kayen, R. E., B. A. Carkin, T. Allen, C. Collins, A. McPherson, and D. Minasian (2015). Shear-wave velocity and site-amplification factors for 50 Australian sites determined by the spectral analysis of surface waves method, U.S. Geological Survey Open-File Report 2014–1264, pp 118, doi: 10.3133/ofr20141264.

King, T.R., Quigley, M., and Clark, D. (2019). Surface-rupturing historical earthquakes in Australia and their environmental effects: New insights from re-analyses of observational data: Geosciences, v. 9, no. 10, p. 408, https://doi .org/10.3390/geosciences9100408.

Kottke, A. (2018, July 27). arkottke/pyrotd v0.5.4 (Version v0.5.4). Zenodo. http://doi.org/10.5281/zenodo.1322849

Leonard, M. (2010). Earthquake Fault Scaling: Self-Consistent Relating of Rupture Length, Width, Average Displacement, and Moment Release. *Bull. Seis. Soc. Am,* 100, 1971-88.

Leonard, M. (2014). Self-Consistent Earthquake Fault-Scaling Relations: Update and Extension to Stable Continental Strike-Slip Faults. *Bull. Seis. Soc. Am,* 104 (6): 2953–2965. doi: https://doi.org/10.1785/0120140087

Maechling, P. J., F. Silva, S. Callaghan, and T. H. Jordan (2015). SCEC Broadband Platform: System Architecture and Software Implementation, Seismol. Res. Lett., 86, no. 1

McPherson, A. A. (2017). A revised seismic site conditions map for Australia, Geoscience Australia Record 2017/12, Canberra, doi: 10.11636/Record.2017.012.

Saikia, C.K., P.G. Somerville, H.K. Thio, N.F. Smith, A. Pitarka, B.B. Woods (1998). Crustal structure and ground motion models in the eastern and Central United States from National Seismograph Network Data. NUREG/CR-6593, U.S. Nuclear Regulatory Commission.

Seyhan, E., and Stewart, J. P. (2014). Semi-empirical nonlinear site amplification from NGA- West2 data and simulations, Earthquake Spectra 30, 1241–1256.

Somerville, P.G., R.W. Graves, N.F. Collins, S.G. Song, S. Ni and P. Cummins (2009). Source and ground motion models of Australian earthquakes. Proceedings of the 2009 Annual Conference of the Australian Earthquake Engineering Society, Newcastle, Dec 11-13.
Somerville, P. and S. Ni (2010). Contrast in Seismic Wave Propagation and Ground Motion Models between Cratonic and Other Regions of Australia. In Proceedings of the Australian Earthquake Engineering Society, 2010 Conference.
Stewart, J. P., G.A. Parker, G.M. Atkinson, D.M. Boore, Y.M.A. Hashash, and W.J. Silva (2020). Ergodic site amplification model for central and eastern North America. Earthquake Spectra 36 (1), 42-68.
Tan, Y., A Song, S Wei, D Helmberger (2010) Surface Wave Path Corrections and Source Inversions in Southern California. Bulletin of the Seismological Society of America; 100 (6): 2891–2904. doi: https://doi.org/10.1785/0120090063
Wells DL and Coppersmith KJ (1994). New empirical relationships among magnitude, rupture length, rupture width, rupture area, and surface displacement. Bulletin of the Seismological Society of Americ; 84 (4): 974–1002. doi: https://doi.org/10.1785/BSSA0840040974
Yang, H., M. Quigley and T. King (2021). Surface slip distributions and geometric complexity of intraplate reverse-faulting earthquakes. GSA Bulletin; Month/Month 2020; 0; p. 1–21; https://doi.org/10.1130/B35809.1.
Zhao, L. S., and D. V. Helmberger (1994). Source estimation from broadband regional seismograms, Bull. Seismol. Soc. Am., 84, 91–104.